

Magnetic Order in the Double Exchange Model in Infinite Dimensions

Kentaro NAGAI¹, Tsutomu MOMOI^{1,2} and Kenn KUBO³

¹*Institute of Physics, University of Tsukuba, Tsukuba, Ibaraki 305-8571, Japan*

²*Lyman Laboratory of Physics, Harvard University, Cambridge, MA 02138, USA*

³*Department of Physics, Aoyama Gakuin University, Setagaya, Tokyo 157-8572, Japan*

(Received)

We studied magnetic properties of the double exchange (DE) model with $S = 1/2$ localized spins at $T = 0$, using exact diagonalization in the framework of the dynamical mean field theory. Obtained phase diagram contains ferromagnetic, antiferromagnetic and paramagnetic phases. Comparing the phase diagram with that of the DE model with classical localized spins, we found that the quantum fluctuations of localized spins partly destabilize the ferromagnetism and expand the paramagnetic phase region. We found that phase separations occur between the antiferromagnetic and paramagnetic phases as well as the paramagnetic and ferromagnetic ones.

KEYWORDS: double exchange model, infinite dimensions, quantum effect, phase diagram, ferromagnetism, antiferromagnetism, phase separation, density of states

§1. Introduction

Recently perovskite manganese oxides doped with divalent alkaline metals, such as $\text{La}_{1-x}\text{Sr}_x\text{MnO}_3$ and $\text{La}_{1-x}\text{Ca}_x\text{MnO}_3$, are studied extensively.¹⁾ In these materials the decrease of $3d$ electrons caused by the doping with divalent metals leads to drastic changes of magnetic and transport properties. For example, the mother material LaMnO_3 is insulating and has an antiferromagnetic (AF) order at low temperatures. This AF insulator is transformed to a ferromagnetic (F) one by doping, and the F state becomes metallic for $x \gtrsim 0.20$.²⁾ The orthorhombic crystal structure changes into a rhombohedral one with higher symmetry in the metallic phase. The so-called colossal negative magneto-resistance shown by these materials is attracting intense interests due to its potential applications.³⁾

Zener proposed the double exchange (DE) mechanism, which describes essential physics in these materials.⁴⁾ In this paper we study the simplest model that contains this mechanism, i.e. the DE model. In this model three t_{2g} electrons on a Mn ion are treated as a localized spin and the two-fold degeneracy of e_g orbitals is neglected. The Hamiltonian is defined as

$$H = -t \sum_{\langle i,j \rangle, \sigma} c_{i\sigma}^+ c_{j\sigma} - J_H \sum_i \mathbf{S}_i \cdot \mathbf{s}_i. \quad (1.1)$$

Here t denotes the hopping amplitude between the nearest neighbor sites, $c_{i\sigma}$ ($c_{i\sigma}^+$) the annihilation (creation) operator of an e_g electron at the site i with spin σ , and \mathbf{S}_i and \mathbf{s}_i are the localized spin and the spin of the e_g electron at the site i , respectively. Itinerant e_g electrons are assumed to occupy a single orbital and interact with the localized spins through the Hund coupling J_H .

Anderson and Hasegawa⁵⁾ showed that in the limit of strong Hund coupling the hopping amplitude of electrons between the sites i and j is reduced as $\tilde{t}_{ij} = t \cos(\theta_{ij}/2)$ when the angle between the localized spins \mathbf{S}_i and \mathbf{S}_j is θ_{ij} . The hopping amplitude is largest when $\theta_{ij} = 0$, which implies that the F state minimizes the kinetic energy. This is the DE mechanism for the ferromagnetism proposed by Zener.⁴⁾ The competition between the DE mechanism and the antiferromagnetic super-exchange interactions between the localized spins was studied by de Gennes.⁶⁾ Kubo and Ohata studied the DE model in the strong coupling limit.⁷⁾

Recently Furukawa studied this model with classical localized spins using the dynamical mean field theory (DMFT), which is exact in infinite dimensions.⁸⁻¹¹⁾ In DMFT the effective action for the system is equivalent to that for a single impurity problem, and the momentum dependence is absent in the self-energy of the one-particle Green function. These features of the DMFT make the calculations of various properties tractable. He obtained the thermodynamic as well as the transport properties of the model employing a semicircular as well as a Lorentzian density of states for non-interacting electrons. The DE model with classical spins was studied also in finite dimensions with numerical methods. Owing to these studies the properties of the DE model with classical localized spins are fairly well understood. The DE model with quantum localized spins is also studied. The spin wave spectrum¹²⁾ and the ground state phase diagram^{13, 14)} in one and two dimensions were studied by numerical diagonalization. Variational arguments^{15, 16)} show that the fully polarized state is destabilized in a certain density region even in the strong coupling limit. Electronic states were also studied by a many-body CPA

approximation.¹⁷⁾ Due to the difficulty of the strong correlation effects, we have still much to understand the effects of quantum fluctuations in the DE model.

In this paper, we study the DE model in the cases of $S = 1/2$ and the classical (the limit $S = \infty$ with finite $J_H S$) localized spins in infinite dimensions. Comparing the magnetic phase diagrams in both cases, we clarify the influence of the quantum fluctuations of the localized spins on the magnetic ordering. We use the exact diagonalization method in the framework of the DMFT in order to study the case of $S = 1/2$. We employ the Gaussian density of states for non-interacting electrons, which is exact for the simple hypercubic lattice in infinite dimensions,

$$D_0(\epsilon) = \frac{1}{\sqrt{2\pi}} \exp\left(-\frac{\epsilon^2}{2}\right). \quad (1.2)$$

The contents of this paper are as follows: In section 2 we summarize the method of studying the DE model in infinite dimensions. In section 3 we report the phase diagram and the magnetic susceptibility for the case of $S = \infty$. In section 4 we show the results for the case of $S = 1/2$ and compare them with those for $S = \infty$. In section 5 we summarize the results and give perspectives for future study.

§2. Method

We employed the DMFT to study the DE model (1) in infinite dimensions. Though the method is now a standard one,¹⁸⁾ we briefly describe it in this section for readers who are not familiar with the method. In infinite dimensions, the influence from neighboring sites can be replaced with a dynamical mean field (Weiss field). The problem is hence reduced to a single impurity problem in the Weiss field. The self-energy of the Green function does not depend on the momentum.^{19, 20)} The Green function is written as

$$G_\sigma(\mathbf{k}, i\omega_n) = \frac{1}{i\omega_n - \epsilon_{\mathbf{k}} - \mu - \Sigma_\sigma(i\omega_n)}, \quad (2.1)$$

where $\Sigma_\sigma(i\omega_n)$ is the self-energy and σ denotes the spin suffix. It depends on the momentum \mathbf{k} only through $\epsilon_{\mathbf{k}}$. In the following text we omit the variables \mathbf{k} , $i\omega$ and σ in G , Σ etc. for simplicity. The effective action of the DE model at a temperature $T = \beta^{-1}$ is

$$\begin{aligned} \mathcal{S} = & - \sum_\sigma \int_0^\beta d\tau_1 \int_0^\beta d\tau_2 \Psi_\sigma^*(\tau_1) \mathcal{G}_{0\sigma}^{-1}(\tau_1 - \tau_2) \Psi_\sigma(\tau_2) \\ & - J_H \int_0^\beta d\tau \mathbf{S}(\tau) \cdot \mathbf{s}(\tau), \end{aligned} \quad (2.2)$$

where $\Psi_\sigma^*(\tau)$ and $\Psi_\sigma(\tau)$ are Grassmann variables representing the electrons at the impurity site, $\mathbf{S}(\tau)$ the impurity localized spin, and \mathcal{G}_0^{-1} is the Weiss function that represents a time-dependent mean field. This Weiss function is related to the Green function G and the self-energy Σ as $\mathcal{G}_0^{-1} = G^{-1} - \Sigma$.

We obtain the Weiss function \mathcal{G}_0 and the Green function G self-consistently through the following procedures.

- A. Given \mathcal{G}_0^{-1} , then calculate G employing the effective action.
- B. Calculate Σ from G through the relation $\mathcal{G}_0^{-1} = G^{-1} - \Sigma$.
- C. Calculate G from Σ as

$$G(i\omega_n) = \int d\epsilon \frac{D_0(\epsilon)}{i\omega_n - \epsilon - \mu - \Sigma}, \quad (2.3)$$

where $D_0(\epsilon)$ is the density of states given by (1.2).

- D. Obtain \mathcal{G}_0^{-1} again by using $\mathcal{G}_0^{-1} = G^{-1} - \Sigma$.

We repeat the procedures from A to D until a self-consistent solution is obtained.

The main difficulty in these procedures lies in the procedure A, where we must solve a quantum many-body problem. For finite S , we cannot accomplish this procedure exactly and hence we need an approximation. The Weiss function is expressed as

$$\begin{aligned} \mathcal{G}_{0\sigma}(i\omega_n)^{-1} &= i\omega_n + \mu + \int_{-\infty}^{\infty} d\omega' \frac{\Delta_\sigma(\omega')}{i\omega_n - \omega'} \\ &= i\omega_n + \mu + \sum_{p=2}^{\infty} \frac{V_{p\sigma}^2}{i\omega_n - \tilde{\epsilon}_{p\sigma}}, \end{aligned} \quad (2.4)$$

where $\Delta_\sigma(\omega) = \sum_p V_{p\sigma}^2 \delta(\omega - \tilde{\epsilon}_{p\sigma})$. In this study we approximate $\mathcal{G}_{0\sigma}(i\omega_n)$ with $\mathcal{G}_{0\sigma}^{N_S}(i\omega_n)$ which is the Weiss function for a finite number of discrete orbitals;

$$\mathcal{G}_{0\sigma}^{N_S}(i\omega_n)^{-1} = i\omega_n + \mu + \sum_{p=2}^{N_S} \frac{V_{p\sigma}^2}{i\omega_n - \tilde{\epsilon}_{p\sigma}}. \quad (2.5)$$

The parameters $V_{p\sigma}$ and $\tilde{\epsilon}_{p\sigma}$ are determined self-consistently as to minimize

$$R = \frac{1}{n_{\max} + 1} \sum_{n=0}^{n_{\max}} |\mathcal{G}_0(i\omega_n)^{-1} - \mathcal{G}_0^{(N_S)}(i\omega_n)^{-1}|, \quad (2.6)$$

where n_{\max} labels the maximum frequency employed in the calculation. When the Weiss function is approximated as above, the problem is identical to solve the following impurity Anderson Hamiltonian,

$$\begin{aligned} \mathcal{H} = & \sum_{p \geq 2, \sigma} \tilde{\epsilon}_{p\sigma} a_{p\sigma}^+ a_{p\sigma} + \sum_{p \geq 2, \sigma} V_{p\sigma} (a_{p\sigma}^+ d_\sigma + d_\sigma^+ a_{p\sigma}) \\ & + \epsilon_d \sum_\sigma d_\sigma^+ d_\sigma - J_H \mathbf{S} \cdot \mathbf{s}, \end{aligned} \quad (2.7)$$

where $a_{p\sigma}^+$ ($a_{p\sigma}$) and d_σ^+ (d_σ) are the creation (annihilation) operators of the orbital p and the impurity site, respectively, and $s^\alpha = \frac{1}{2} \sum_{\sigma, \sigma'} d_\sigma^+ \sigma_{\sigma, \sigma'}^\alpha d_{\sigma'}$. We obtain the ground state of this Hamiltonian with use of the exact diagonalization method, and calculate the Green function. The kinetic and interaction energies in the ground

state $|\text{G.S.}\rangle$ are obtained with use of the expressions,²¹⁾

$$E_{\text{kin}} = \langle \text{G.S.} | \sum_{p \geq 2, \sigma}^{N_S} V_p (a_{p\sigma}^+ d_\sigma + d_\sigma^+ a_{p\sigma}) | \text{G.S.} \rangle \quad (2.8)$$

and

$$E_{\text{int}} = \langle \text{G.S.} | -J_{\text{H}} \mathbf{S} \cdot \mathbf{s} | \text{G.S.} \rangle. \quad (2.9)$$

Although the size of a localized spin is $3/2$ in actual manganese oxides, we adopt the case of $S = 1/2$ in order to emphasize the quantum effects as well as for simplicity. The approximation improves with increase of the number $N_S - 1$ of the assumed orbitals. The present study was restricted to $N_S \leq 8$ due to technical reasons.

We also calculate the case of $S = \infty$ for the sake of comparison. In this case the procedure A is easily accomplished because the effective action is that of non-interacting electrons. The partition function in the case of $S = \infty$ is given by

$$Z = \int d\Omega_{\mathbf{S}} \int \prod_{\sigma} \mathcal{D}\Psi_{\sigma}^* \mathcal{D}\Psi_{\sigma} \exp(-\mathcal{S}(\mathbf{S})) \quad (2.10)$$

with

$$\begin{aligned} \mathcal{S}(\mathbf{S}) = & \sum_{\sigma} \int_0^{\beta} d\tau_1 \int_0^{\beta} d\tau_2 \Psi_{\sigma}^*(\tau_1) \mathcal{G}_{0\sigma}^{-1}(\tau_1 - \tau_2) \Psi_{\sigma}(\tau_2) \\ & - J_{\text{H}} \int_0^{\beta} d\tau \mathbf{S} \cdot \mathbf{s}(\tau), \end{aligned} \quad (2.11)$$

where \mathbf{S} is a classical vector of size S and $\Omega_{\mathbf{S}}$ denotes the volume angle of the direction of the localized spin. The Green function is given by

$$G_{\sigma}(i\omega_n) = \frac{1}{Z} \int d\Omega_{\mathbf{S}} P(\mathbf{S}) (\mathcal{G}_{0\sigma}^{-1}(i\omega_n) + J_{\text{H}} \mathbf{S} \cdot \mathbf{s}(i\omega_n))^{-1}, \quad (2.12)$$

where $P(\mathbf{S})$ is the Boltzmann weight for the configuration of the localized spin,

$$P(\mathbf{S}) = \int \prod_{\sigma} \mathcal{D}\Psi_{\sigma}^* \mathcal{D}\Psi_{\sigma} \exp(-\mathcal{S}(\mathbf{S})). \quad (2.13)$$

§3. Results for $S = \infty$

In this section we report the temperature dependence of the magnetic susceptibility and the phase diagram at a very low temperature in the case of $S = \infty$.

In infinite dimensions the susceptibility depends on the wave vector \mathbf{q} only through $X(\mathbf{q})$,²⁰⁾ where $X(\mathbf{q})$ is defined by

$$X(\mathbf{q}) = \frac{1}{d} \sum_{i=1}^d \cos q_i. \quad (3.1)$$

Here d denotes dimensionality of the space. The F and AF susceptibilities correspond to the cases with $X(\mathbf{q}) = 1.0$ and -1.0 , respectively, and a case where $-1.0 < X(\mathbf{q}) < 1.0$ corresponds to an incommensurate order. Figure 1 shows the magnetic susceptibility

χ for $J_{\text{H}}S = 5.0$ at the electron density $n = 1.0$. Figure 1(a) exhibits the wave-vector dependence of the susceptibility at various temperatures. The susceptibility has maximum at $X(\mathbf{q}) = -1.0$ at all temperatures and it increases with decrease of temperature. In Fig. 1(b) the inverse of the AF susceptibility is shown as a function of temperature. The susceptibility obeys the Curie-Weiss law and diverges at a finite temperature T_N . As a result the AF order is expected to appear at temperatures below $T_N \cong 0.044$ for $J_{\text{H}}S = 5.0$ and $n = 1.0$. Next, the susceptibility for $J_{\text{H}}S = 5.0$ and $n = 0.8$ is shown in Fig. 2. In this case the F susceptibility is largest, and obeys the Curie-Weiss law. The F order is expected to appear at temperatures below $T_C \cong 0.062$.

We obtained a phase diagram at a very low temperature ($\beta = 400$) assuming the uniform or a two sublattice structure. The result is shown in Fig. 3, where the AF, F and paramagnetic (P) phases are present. For $n = 1$ the AF state is stable for any positive J_{H} . The AF phase spreads out to a small region close to the line $n = 1$ for weak Hund coupling.

The F phase occupies a large region where $n \lesssim 0.5$ and $J_{\text{H}}S \gtrsim 1$. This F state has almost fully polarized magnetization. In Fig. 4, we show the spontaneous magnetization for $n = 0.4$ at $\beta = 400$ as a function of $J_{\text{H}}S$. The magnetization starts increasing continuously at $J_{\text{H}}S \cong 0.9$ and rapidly approaches the limiting value of $0.98m_0$ where m_0 is the value of the full polarization. In this case the transition to the F state is of the second order. The P phase appears for $J_{\text{H}}S \lesssim 3$ and it spreads to a wide density region for weak coupling. Phase separation (PS) occurs between the AF and P phases for $J_{\text{H}}S \lesssim 3$ and also between the AF and F phases for $J_{\text{H}}S \gtrsim 3$. General features of the phase diagram is similar to those obtained previously in infinite dimensions^{14, 22)} and roughly understood as a result of the competition between the AF coupling, which is a second order effect of the hopping, and the ferromagnetic DE mechanism. Since the AF coupling decreases with increasing $J_{\text{H}}S$ as $t^2/J_{\text{H}}S$, the relative strength of the F coupling, which is proportional to t , increases with J_{H} . Occurrence of the PS for small doping ($n \simeq 1$) may be understood as the instability of a canted AF state.²³⁾

Since we assumed a two-sublattice structure there remains the possibility that we missed magnetic phases with more complicated spatial structures, e.g. those with incommensurate (IC) wave vectors. Such IC order was predicted previously to occur for intermediate doping.^{22, 24)} The obtained P phase might be an IC phase in reality. In fact we found the cases where χ corresponding to an IC order diverges at higher temperatures. Figure 4 shows χ for $J_{\text{H}}S = 1.0$, $n = 0.66$ and $\beta = 110$. We observe a sharp maximum of χ at $X(\mathbf{q}) \simeq -0.9$ and it diverges at a critical temperature. It is certain that an IC phase exists below the critical temperature. Study of the phase diagram which contains IC phases is left for a

future study.

§4. Results for $S = 1/2$

Quantum Monte Carlo method is usually used in the framework of the DMFT for studying the thermodynamic properties at finite temperatures.¹⁸⁾ This method, however, suffers from a serious negative-sign problem in the study of the DE model with quantum localized spins.²⁵⁾ In this section, we therefore studied only the ground state properties for the model with $S = 1/2$ localized spins, employing the exact diagonalization technique. We report the results and compare them with those for the case of $S = \infty$.

Figures 6(a) and 6(b) show the ground state phase diagram obtained with $N_S = 6$ and 8, respectively. We should extrapolate the results of finite N_S to the limit $N_S = \infty$ in order to obtain the exact result. We observe that the two phase diagrams are almost same except for the boundary of the F phase. Difference between results for $N_S = 6$ and 8 is still large on the boundary of the F phase and hence the obtained boundary may not represent that of $N_S = \infty$ correctly. Nevertheless these results exhibit contrast to that for the case of $S = \infty$ in several points.

The AF phase appears in a region close to the line $n = 1$ and its boundaries for $N_S = 6$ and 8 agree very well. It is remarkable that the AF phase is much more stabilized for $S = 1/2$ than for $S = \infty$ in the weak coupling region. It extends to $n \simeq 0.7$ and, as a result, the region of PS narrows for small J_H in contrast to the result for $S = \infty$. The present result shows that the AF phase is stable for $0.8 \lesssim n \leq 1$ even for $J_H = 0.1$, the smallest J_H studied, though the system should be paramagnetic for all $0 < n < 1$ for $J_H = 0$.

The F phase appears for $J_H S \gtrsim 4$ in a wide range of the density, i.e., $n \lesssim 0.7$. Results for $N_S = 6$ and 8 agree well in this region. On the other hand, the F phase is strongly reduced for $J_H S \lesssim 3$ by increasing N_S and almost disappears for $J_H S \lesssim 1$ in Fig. 6(b). In comparison with the $S = \infty$ case, the F phase region for $N_S = 8$ is fairly reduced. We may need further study with larger N_S to confirm this strong reduction of the F phase.

Between the AF and F phases we obtain a P phase in a wide density range, and PS occurs between the AF and F phases as well as between the P and F phases. The P phase persists to large J_H , i.e. $J_H S \simeq 5$ in contrast to the case of $S = \infty$ where the P phase terminates at $J_H S \simeq 3$. We should note that the obtained P phase might be replaced by phases with more complicated spatial structures, e.g. IC phases, in more comprehensive calculations, which include larger-sublattice structures.

Figure 6 shows the electron density n as a function of the chemical potential μ for $J_H S = 5.0$ and $N_S = 8$. We see jumps of n at two values of μ , which indicate the occurrence of PS's. The density region of the PS

between the AF and P phases narrows with decreasing J_H in contrast to the case of $S = \infty$. This is caused by the expansion of the AF phase in the weak coupling region. The PS occurs in a very narrow density region between the P and F phases for $J_H S \gtrsim 2$. This PS was not found in the case of $S = \infty$.

In Figs. 7(a) and 7(b), we show the kinetic energy and the magnetization of conduction electrons, respectively, as functions of $J_H S$ for $n = 0.4$. The kinetic energy [Fig. 8(a)] increases with J_H very rapidly in the P phase, while it shows a saturation in the F phase for $J_H S \geq 3.5$. This behavior is a characteristic of the ferromagnetism caused by the DE mechanism and indicates that the scattering by the Hund coupling ceases to be operative by alignment of the localized spins.²⁶⁾ In Fig. 8(b), the F phase starts with a finite magnetization at $J_H S = 3.5$, which indicates a first-order transition from the P phase. The occurrence of PS between the F and P phases is related to the first-order character of the phase transition. The magnetization increases with J_H and apparently approaches to a finite value nearly equal to $0.6m_0$, where m_0 denotes the magnetization of a fully polarized state. It is noticeable that the saturated moment is relatively small in comparison with the result for the $S = \infty$ localized spins. This result gives evidence that the quantum fluctuations of the localized spins destabilize ferromagnetism. Though the fully polarized state cannot be realized for the Gaussian density of states, the reduction of the magnetization mostly comes from the quantum fluctuations of the localized spins.

We also studied the electronic states in the ground states. The local density of states (DOS) is calculated from the Green function obtained in the procedure A in section 2. Because we treat the system with a finite number of discrete orbitals, the obtained DOS is composed of finite number of sharp peaks. Figures 9(a-d) exhibit examples of the DOS obtained by calculations with $N_S = 8$, where an artificial imaginary part $0.1i$ is added to $\Sigma(\omega)$ for the purpose of illustration. Figure 9(a) exhibits the local DOS in an AF ground state for $J_H S = 5.0$ at $n = 1.0$. We can observe characteristic features of the DOS in the AF ground state in the strong coupling region (in spite of the discretized structures due to the approximation). In this case DOS is composed of two sub-bands each of which corresponds to electronic states with parallel and antiparallel spins with localized spins. Two sub-bands are separated from the Fermi level by a broad energy gap, which indicates that the ground state is insulating. The lower DOS for up spin has a large weight compared to that for down spin, since spin is almost fully polarized upwards on this site. Figure 9(b) shows the local DOS of a F ground state for $J_H S = 5.0$ at $n = 0.78$. Also in this case the DOS is composed of two sub-bands separated by an energy gap (the main part of the upper sub-band is out of range of the figure). The Fermi level is inside of the lower sub-bands,

which indicates the metallic partially polarized ground state. The DOS for down spin is much smaller than that for up spin, which implies that the spins are polarized upwards. The width of the lower sub-bands for both spins are almost same, which reflects the mixing due to exchange scattering. The DOS in the AF ground state for $J_H S = 0.5$ at $n = 1.0$ is exhibited in Fig. 9(c). In this case the DOS is apparently composed of a single band centered around the Fermi level. It is expected that there is an energy gap caused by the AF order and/or Umklapp scatterings. However it is exhibited as a dip at the Fermi level. This is only due to the width added artificially. The DOS for down spin below Fermi level is smaller than, but comparable to that for up spin due to small sublattice magnetization. We show in Fig. 9(d) the DOS for $J_H S = 0.5$ and $n = 0.73$ where the ground state is antiferromagnetic. In this case the dip located at $\epsilon = \mu + 0.3$ may correspond to the gap due to the AF ordering. The Fermi level lies very close to the top of a peak. These results suggest that the ground state is a metallic state with AF long range order.

§5. Summary and future work

We studied the DE model with $S = 1/2$ as well as $S = \infty$ localized spins in infinite dimensions with use of the DMFT. It is found that quantum fluctuations of localized spins partly destabilize the ferromagnetic ground state and the paramagnetic phase expands in the case of $S = 1/2$. The F state for $S = 1/2$ has rather small polarization even for a strong coupling, such as $J_H S \gtrsim 5.0$. This is in contrast to the results for $S = \infty$, where the ground states were almost fully polarized.^{14, 22)} On the other hand the AF ground state is stabilized by quantum effects for weak coupling. A similar result was recently reported for a model with degenerate orbitals.²⁷⁾ It is interesting to examine whether these results still hold for different choice of DOS (for non-interacting electrons) from the Gaussian one.

More accurate calculations to determine the precise ground state phase diagram is left for a future study. The obtained phase diagrams for the $S = 1/2$ localized spin systems do not show good convergence at the boundary of the ferromagnetic phase. Furthermore the ground state was obtained under the assumption of the two-sublattice structure. We found that the phase transition to an IC state occurs in the case of $S = \infty$ and we expect it to occur for $S = 1/2$ as well.

It is interesting to study the case of $S = 3/2$ and compare the result with those for $S = 1/2$ and ∞ , since the magnitude of the localized spins are $3/2$ in real manganites. This is now under progress and will be reported elsewhere.

§6. Acknowledgements

The authors are indebted to D.M. Edwards, A.C.M. Green, T.A. Kaplan, N. Furukawa, D.S. Hirashima and

H. Tsunetsugu for valuable discussions and helpful comments. This work was supported by Grant in Aid Nos. 09640453 and 11640365 from the Ministry of Education, Science and Culture of Japan. Numerical calculations were done on Facom VPP500 at the ISSP of the University of Tokyo.

- 1) For references, *Physics of Manganites*, eds. by T.A. Kaplan and S.D. Mahanti, (Kluwer Academic/Plenum Publ., New York, 1999), and papers cited therein.
- 2) G.H. Jonker and J.H. Van Santen, *Physica* **16**, 337 (1950); J.H. Van Santen and G.H. Jonker, *ibid.* page 599.
- 3) K. Chahara, T. Ohno, M. Kasai and Y. Kozono, *Appl. Phys. Lett.* **63**, 1990 (1993); S. Jin, T.H. Tiefel, M. McCormack, R.A. Fastnacht, R. Ramesh and L.H. Chen, *Science*, **264**, 413 (1994); A. Urushibara, Y. Moritomo, T. Arima, A. Asamitsu, G. Kido and Y. Tokura, *Phys. Rev. B* **51**, 14103 (1994).
- 4) C. Zener, *Phys. Rev.* **82**, 403 (1951).
- 5) P. W. Anderson and H. Hasegawa, *Phys. Rev.* **100**, 675 (1955).
- 6) P. G. de Gennes, *Phys. Rev.* **118**, 141 (1960).
- 7) K. Kubo and N. Ohata, *J. Phys. Soc. Jpn.* **33**, 21 (1972).
- 8) N. Furukawa, in *Physics of Manganites*, eds. by T.A. Kaplan and S.D. Mahanti, (Kluwer Academic/Plenum Publ., New York, 1999) p.1, and papers cited therein.
- 9) N. Furukawa, *J. Phys. Soc. Jpn.* **63**, 3214 (1994).
- 10) N. Furukawa, *J. Phys. Soc. Jpn.* **64**, 2754 (1995).
- 11) N. Furukawa, *J. Phys. Soc. Jpn.* **65**, 1174 (1996).
- 12) J. Zang, H. Röder, A.R. Bishop and S.A. Trugman, *J. Phys. Condens. Matter* **9**, L157 (1997); T.A. Kaplan and S.D. Mahanti, *J. Phys. Condens. Matter* **9**, L291 (1997); P. Wurth and E. Müller-Hartmann, *Eur. Phys. J. B* **5**, 403 (1998); D.I. Golosov, preprint cond-mat/9908202.
- 13) J. Riera, K. Hallberg and E. Dagotto, *Phys. Rev. Lett.* **79**, 713 (1997).
- 14) E. Dagotto, S. Yunoki, A. Malvezzi, A. Moreo, J. Hu, S. Capponi, D. Poilblanc and N. Furukawa, *Phys. Rev. B* **58**, 6414 (1998).
- 15) T. Okabe, *Prog. Theor. Phys.* **97**, 21 (1997); *ibid.* **98**, 331 (1997).
- 16) R. E. Brunton and D. M. Edwards, *J. Phys. Condens. Matter* **10**, 5421 (1998).
- 17) D.M. Edwards, A.C.M. Green and K. Kubo, *J. Phys. Condens. Matter* **11**, 2791 (1999).
- 18) For reviews see D. Vollhardt, in *Correlated Electron Systems*, Vol.9, ed. by V.J. Emery (World Scientific, Singapore, 1993) p.57; A. Georges, G. Kotliar, W. Krauth and M.J. Rozenberg, *Rev. Mod. Phys.* **68**, 13 (1996).
- 19) W. Metzner and D. Vollhardt, *Phys. Rev. Lett.* **62**, 324 (1989).
- 20) E. Müller-Hartmann, *Z. Phys. B* **76**, 211 (1989); *ibid.* **74**, 507 (1989).
- 21) M. J. Rozenberg, G. Moeller and G. Kotliar, *Mod. Phys. Lett. B* **8** 535 (1994).
- 22) S. Yunoki, J. Hu, A.L. Malvezzi, A. Moreo, N. Furukawa and E. Dagotto, *Phys. Rev. Lett.* **80**, 845 (1998).
- 23) D.I. Golosov, M.R. Norman and K. Levin, *Phys. Rev. B* **58**, 8617 (1998).
- 24) J. Inoue and S. Maekawa, *Phys. Rev. Lett.* **74**, 3407 (1995).
- 25) K. Nagai, T. Momoi and K. Kubo, unpublished.
- 26) K. Kubo, D. M. Edwards, A.C. M. Green, T. Momoi and H. Sakamoto, in *Physics of Manganites*, eds. by T.A. Kaplan and S.D. Mahanti, (Kluwer Academic/Plenum Publ., New York, 1999) p.71.
- 27) A. Chattopadhyay, A. J. Millis and S. Das Sarma cond-

mat/9908305.

Fig. 1. The magnetic susceptibility χ for $J_H S = 5.0$ and $n = 1.0$.
 (a) Wave-vector dependence of χ . (b) Temperature dependence of the antiferromagnetic susceptibility ($X(\mathbf{q}) = -1.0$). $X(\mathbf{q})$ is defined by (3.1) in the text.

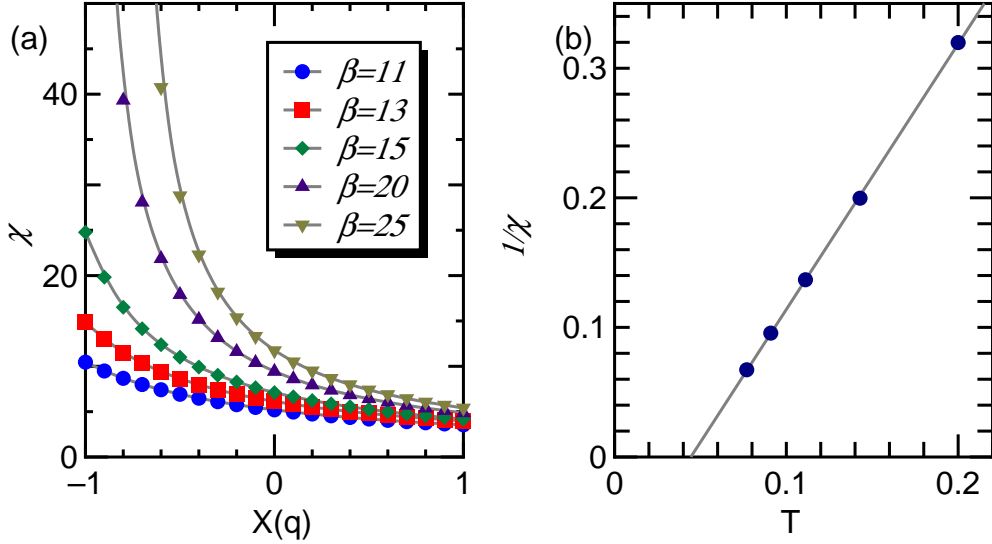


Fig. 2. The susceptibility for $J_H S = 5.0$ and $n = 0.8$. (a) Wave-vector dependence of the susceptibility. (b) Temperature dependence of the ferromagnetic susceptibility ($X(\mathbf{q}) = 1.0$).

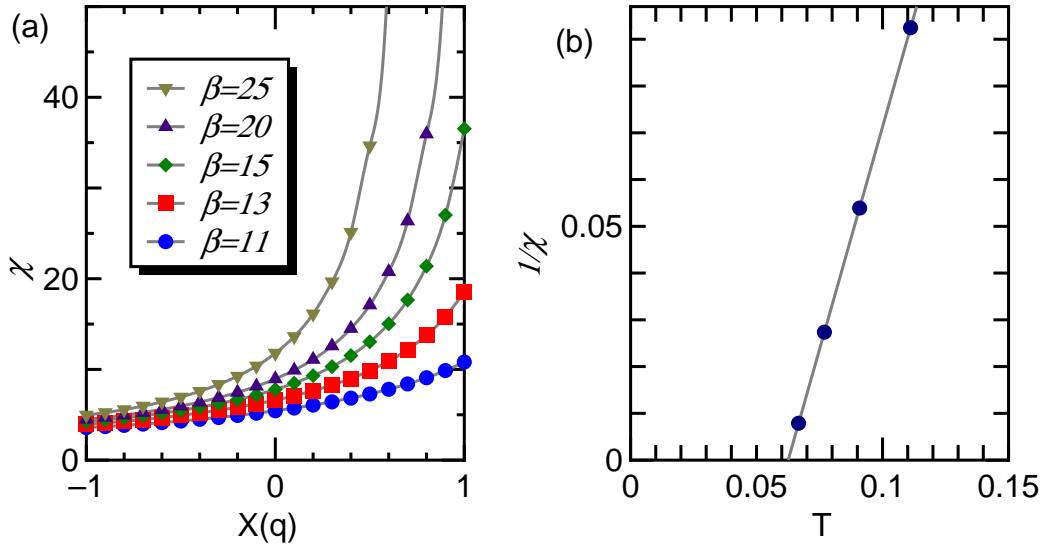


Fig. 3. Phase diagram for $S = \infty$ at $\beta = 400$. Antiferromagnetic, ferromagnetic and paramagnetic phases are denoted by AF, F and P, respectively. PS means the region where phase separation occurs.

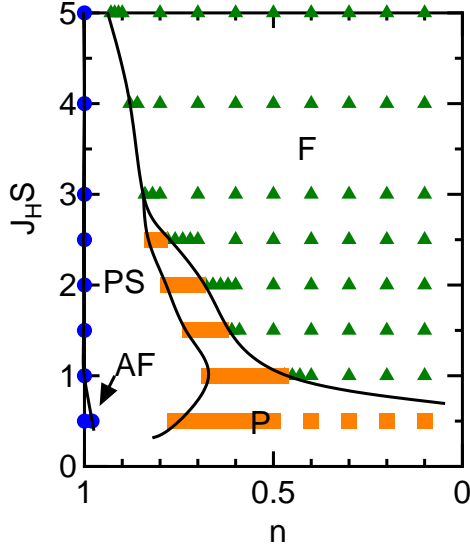


Fig. 4. The magnetization for $S = \infty$, $\beta = 400$ and $n = 0.4$ as a function of $J_H S$.

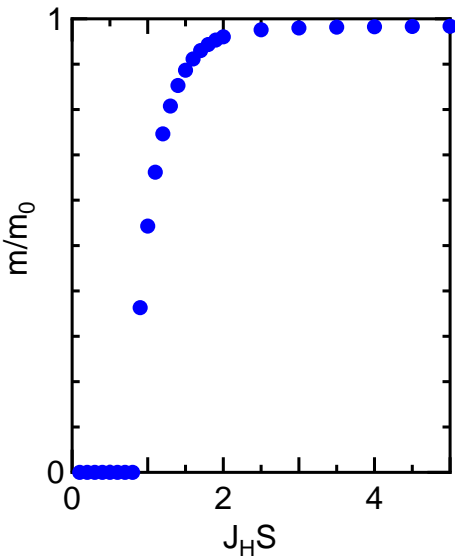


Fig. 5. Wave-vector dependence of the spin susceptibility for $J_H S = 1.0$, $n = 0.66$ and $\beta = 110$.

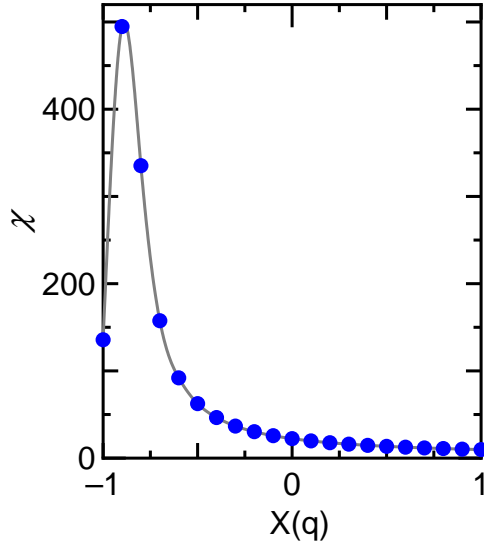


Fig. 6. Phase diagrams of the ground state derived by the exact diagonalization method with $N_S = 6$ (a) and $N_S = 8$ (b). AF, F and P denote antiferromagnetic, ferromagnetic and paramagnetic phases, respectively. PS means the region where phase separation occurs.

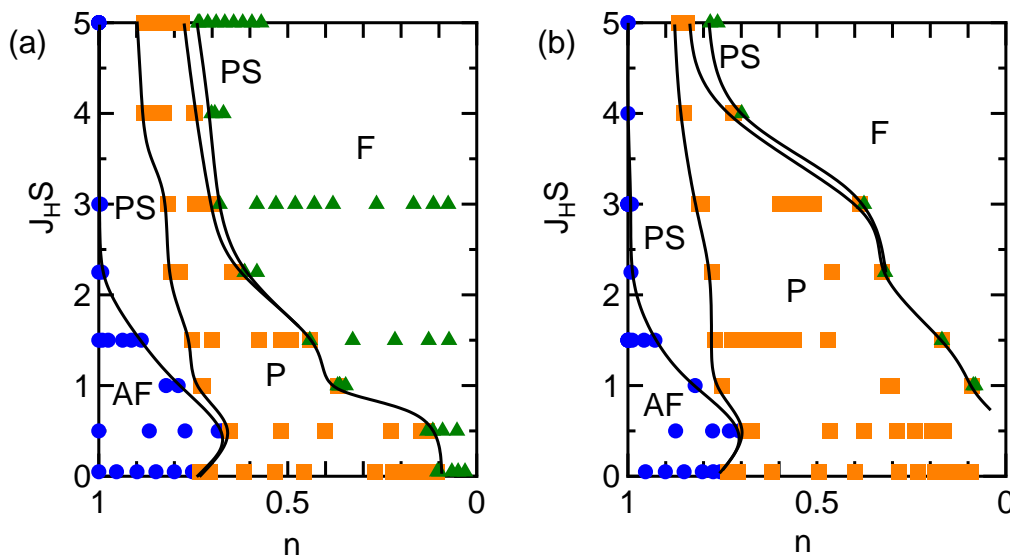


Fig. 7. The electron density n as a function of μ in the ground state for $J_H S = 5.0$ and $N_S = 8$. Circles, squares and triangles indicate the antiferromagnetic, paramagnetic and ferromagnetic states, respectively.

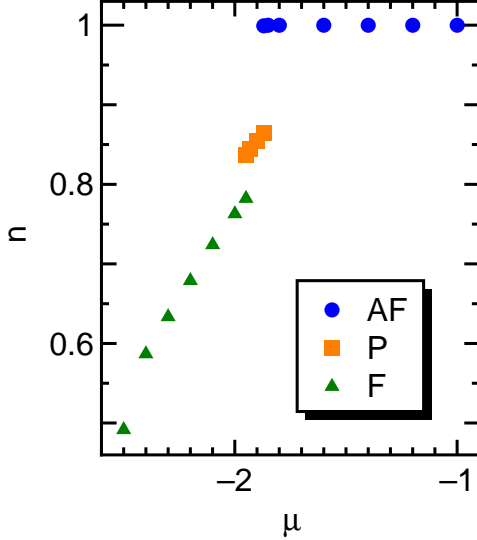


Fig. 8. The kinetic energy (a) and the magnetization (b) of the ground state as functions of $J_H S$ for $n = 0.4$ and $N_S = 8$. Rhombuses and squares indicate the paramagnetic and ferromagnetic states, respectively.

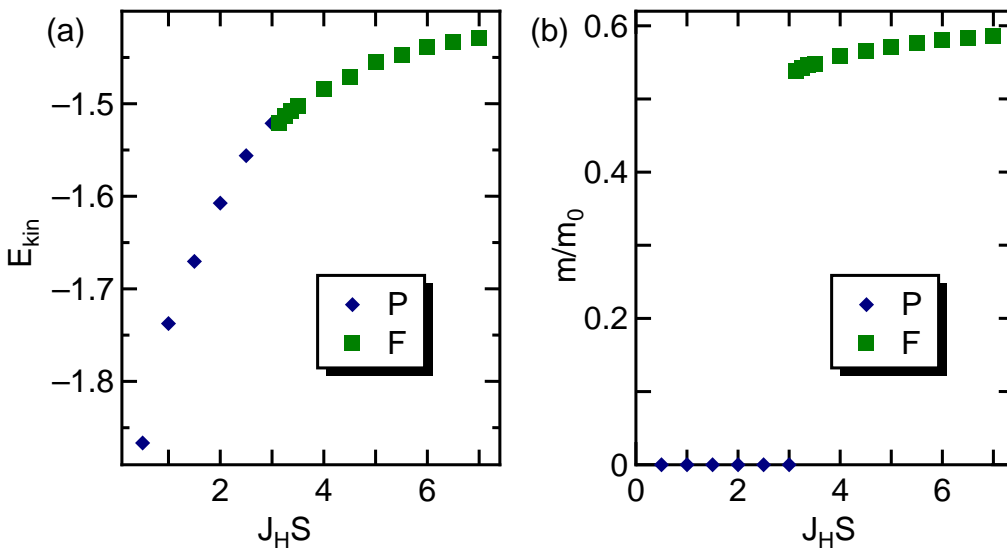


Fig. 9. Density of states for $J_H S = 5.0$ at $n = 1.0$ (a) and $n = 0.78$ (b), and for $J_H S = 0.5$ at $n = 1.0$ (c) and $n = 0.73$ (d).

